Hybrid IPT Topologies With Constant Current or Constant Voltage Output for Battery Charging Applications

Xiaohui Qu, *Member, IEEE*, Hongdou Han, Siu-Chung Wong, *Senior Member, IEEE*, Chi K. Tse, *Fellow, IEEE*, and Wu Chen, *Member, IEEE*

***Abstract*—The inductive power transfer (IPT) technique in battery charging applications has many advantages compared to conventional plug-in systems. Due to the dependencies on transformer characteristics, loading profile, and operating frequency of an IPT system, it is not a trivial design task to provide the battery the required constant charging current (CC) or constant battery charging voltage (CV) efficiently under the condition of a wide load range possibly defined by the charging profile. This paper analyzes four basic IPT circuits with series–series (SS), series–parallel (SP), parallel–series (PS), and parallel–parallel (PP) compensations systematically to identify conditions for realizing load-independent output current or voltage, as well as resistive input impedance. Specifically, one load-independent current output circuit and one load-independent voltage output circuit having the same transformer, compensating capacitors, and operating frequency can be readily combined into a hybrid topology with fewest additional switches to facilitate the transition from CC to CV. Finally, hybrid topologies using either SS and PS compensation or SP and PP compensation are proposed for battery charging. Fixed-frequency duty cycle control can be easily implemented for the converters.**

***Index Terms*—Battery charging, constant current (CC) output, constant voltage (CV) output, inductive power transfer (IPT), resistive input impedance.**

I. Introduction

INDUCTIVE power transfer (IPT) systems using varying magnetic fields to deliver power efficiently have found many applications in electrical vehicle (EV) battery charging [1]–[5], consumer electronics [6]–[9], underwater or mining lighting systems [10]–[12], etc. Compared to conventional plug-in systems, IPT systems realize both electrical and mechanical isolation, minimizes the use of cables and sockets, and ensures safe operation in harsh environments. Specifically in EV battery charging, the IPT primary supply windings can be buried underneath the existing parking space, which eliminates the need for additional charging stations. Moreover, IPT can realize on-the-road EV charging, such that the charging capacity and charging time of EV battery could be reduced simultaneously [5], [13]. Thus, IPT battery charging plays an important role in the development of the EV market.

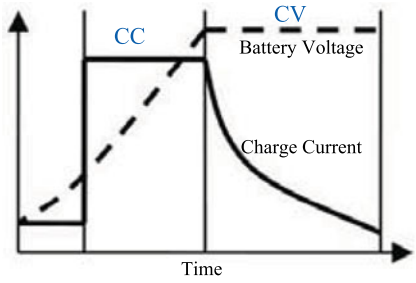

Fig. 1. Typical charge profile of a lithium-ion battery cell.

Recently, high-performance lithium-ion batteries are widely used in EVs and cell phones. Fig. 1 shows the typical charging profile, where the constant current (CC) mode and constant voltage (CV) mode charging are dominant. The charging process starts with the CC mode. The battery voltage increases rapidly. When the battery voltage reaches a specified level, the charger goes into CV mode until the charging current decreases to nearly zero. Considering the battery lifetime and recycle time, an IPT battery charger must provide sufficiently accurate charging current and voltage for safe operation.

It is well known that the loosely coupled transformer in an IPT system has significant leakage inductors. This affects the transfer efficiency and components' ratings. Compensation of reactive power is needed for transfer of real power to the load side. The output voltage and current are thus functions of the transformer parameters, switching frequency, and load impedance. From the charging profile shown in Fig. 1, the battery equivalent resistance increases significantly as the charging operation goes from CC to CV modes. To provide the required output current or voltage efficiently, two basic control methodologies are considered. Pulse width modulation (PWM) control at a fixed frequency could readily compensate the reactive power but it is hard to regulate the output voltage or current under the wide load variation because the corresponding large variation of the duty cycle will not permit zero-voltage switching (ZVS) to be incorporated. Moreover, variable frequency control may achieve the required output current under load variation, but the reactive power can only be partially compensated within a

Manuscript received September 29, 2014; revised December 8, 2014; accepted January 13, 2015. Date of publication January 23, 2015; date of current version July 10, 2015. This work was supported by the National Natural Science Foundation of China under Grant 51107009, by the Natural Science Foundation of Jiangsu Province under Grant BK20141339, and by the Hong Kong RGC General Research Fund under Grant PolyU 5274/13E. Recommended for publication by Associate Editor Y. J. Jang.

X. Qu, H. Han, and W. Chen are with the School of Electrical Engineering, Southeast University, Nanjing 210096, China (e-mail: xhqu@seu.edu.cn; 837936502@qq.com; chenwu@seu.edu.cn).

S.-C. Wong and C. K. Tse are with the Department of Electronic and Information Engineering, Hong Kong Polytechnic University, Hung Hom, Hong Kong (e-mail: enscwong@polyu.edu.hk; encktse@polyu.edu.hk).

Color versions of one or more of the figures in this paper are available online at http://ieeexplore.ieee.org.

Digital Object Identifier 10.1109/TPEL.2015.2396471

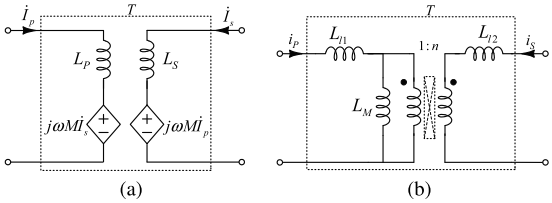

Fig. 2. Equivalent models of loosely coupled transformer T. (a) M model; (b) T model.

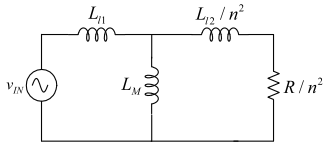

Fig. 3. Equivalent primary circuit of the T model.

small range of operating frequency, and the transfer efficiency and transformer size are hard to optimize. To assure ZVS for a range of load, a combination of PWM and phase-locked loop control can be used to realize ZVS [14]. However, the phase angle has to be designed inductive for the whole range of load, and considerable reactive power is inevitable. In practice, variable frequency control can be used to compensate reactive power, namely, to achieve zero phase angle (ZPA) between the input voltage and the input current, while the output voltage or current regulation is achieved by a back-end converter [6], [15], [16]. Unfortunately, frequency control may pose a stability issue because the frequency for achieving ZPA may not be unique when the load changes [17], [18]. In addition, the current output back-end converter increases the component counts and associated losses.

To simplify the control and optimize the system efficiency, the operating frequency for achieving a load-independent output can be obtained for an IPT system [19]. An efficient IPT converter with CC or CV output operating at some specified frequencies can be derived, and a fixed frequency control can be easily implemented. However, the IPT system with CC or CV output at the specified frequency cannot guarantee input ZPA. For example, the series–series (SS) compensated converter can realize load-independent CV output at two frequencies [20]. However, at these two frequencies, the input impedance is either capacitive or inductive, and the reactive power will impose stresses on the converter's power switches. On the other hand, it is found that load-independent CC output occurs at only one frequency, where the input impedance is purely resistive [21], [22]. Thus, load-independent CC output and ZPA input for the driver switches can be achieved simultaneously. Other topologies may also meet these requirements, e.g., the parallel–parallel (PP) compensation for CC output and ZPA [23], the (series/series–parallel) S/SP with leakage inductor compensation for CV output and ZPA [24], and so on. They can be used as a CC or CV battery charger. However, a systematical analysis is still missing.

The charging profile shown in Fig. 1 shows two modes of charging. The CC and CV modes of charging transit smoothly when the battery voltage reaches a specified value. The work by Huang *et al.* [25] uses SS compensation to realize CC and CV outputs at two different frequencies. Operating in CC mode, ZPA is automatically realized. Operating in CV mode, the input impedance is inductive which facilitates ZVS. However, excessive reactive power will degrade the transfer efficiency and increase circuit VA ratings. The work by Auvigne *et al.* [26] proposes a dual topology with SS and SP transition to realize CC and CV charging, respectively. To realize ZPA at the same operating frequency, the compensation parameters and transformer parameters in these two modes are different, necessitating the use of a more complex circuit involving two capacitors, a center-tapped loosely coupled transformer, and four switches.

This paper systematically analyzes the load-independent voltage or current output and ZPA characteristics of an IPT system based on the four simple IPT topologies corresponding to SS, SP, parallel–series (PS), PP compensations, where the first letter refers to the primary compensation and the second letter refers to the secondary compensation. Utilizing the characteristics of the four simple IPT topologies, an optimal hybrid topology using a single set of transformers, compensation parameters, and switching frequency will be developed with the smallest number of switches for EV battery charging. With this IPT topology, the battery charger can achieve the required CC or CV charging with lowest power ratings of internal power switches as a result of ZPA operation, fixed frequency control, and high efficiency. Finally, an IPT battery charger prototype with 1-A charging current and 15-V cell voltage will be built to verify the analysis in this paper.

Section II gives a detailed analysis of input impedance and output characteristics of an IPT system. Several optimal hybrid topologies suitable for battery chargers are proposed in Section III. The detailed design process and implementation of the system are given. The performance of the proposed battery charger is evaluated in Section IV. Finally, Section V concludes the paper.

II. Fundamental Analysis

To facilitate the analysis, we use two equivalent models to describe the loosely coupled transformer T, namely the M model and the T model, as shown in Fig. 2(a) and (b), respectively. In Fig. 2(a), M is the mutual inductance, L_P and L_S are the primary and secondary self-inductances, whereas in Fig. 2(b), L_M is the magnetizing inductance, the ideal transformer has turns ratio $1:n$, and finally, L_{l1} and L_{l2} are the primary and secondary leakage inductances. The parameters of the two transformer models are related by

$$\begin{aligned} M &= nL_M \\ L_P &= L_{l1} + L_M = L_{l1} + \frac{M}{n} \\ L_S &= L_{l2} + n^2 L_M = L_{l2} + nM, \text{ and} \\ k &= \frac{M}{\sqrt{L_P L_S}}. \end{aligned} \tag{1}$$

A pure sinusoidal ac voltage source $v_{\rm IN}$ with frequency $f_{\rm sw}$ is used to drive the transformer circuit. For simplicity, the

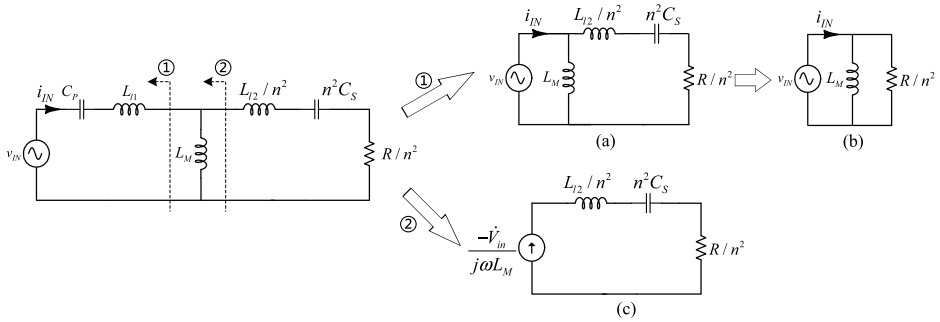

Fig. 4. IPT circuit with SS compensation. Simplified equivalent circuits (a) and (b) for voltage output, and (c) for current output.

secondary circuit of the T model is transformed to an equivalent circuit in the primary as shown in Fig. 3 for subsequent analysis.

A. SS Compensation

Fig. 4 shows an SS compensated IPT circuit, where C_P and C_S are the primary and secondary compensation capacitors, respectively. The values of C_P and C_S are chosen such that

$$\frac{1}{2\pi\sqrt{L_{l1}C_P}} = f_{\rm sw}, \text{ and} \tag{2}$$

$$\frac{1}{2\pi\sqrt{L_{l2}C_S}} = f_{\rm sw}. \tag{3}$$

Thus, the IPT circuit can be simplified to the circuits shown in Fig. 4(a) or (b), where the impedance of an *LC* series resonant circuit vanishes. In Fig. 4(b), the equivalent output voltage in the secondary $nv_{\rm IN}$ is load independent.

If the SS IPT circuit is designed with

$$\frac{1}{2\pi\sqrt{(L_{l1}+L_M)C_P}} = \frac{1}{2\pi\sqrt{L_P C_P}} = f_{\rm sw} \tag{4}$$

then an equivalent current source $v_{\rm IN}/\omega L_M$ is obtained to drive the load, as shown in Fig. 4(c), where $\omega = 2\pi f_{\rm sw}$. The equivalent secondary output current $\dot{I}_o = \frac{1}{n}\cdot -\frac{\dot{V}_{\rm in}}{j\omega L_M} = -\frac{\dot{V}_{\rm in}}{j\omega M}$ is load independent.

To achieve ZPA, the impedance $Z_{\rm IN}$ observed by $v_{\rm IN}$ has to be found at the operating frequency. For applications requiring a load-independent output voltage, the SS IPT circuit using the set of compensations (2) and (3), $Z_{\rm IN}$ is obviously inductive due to the existence of L_M. To compensate L_M, an additional capacitor C_3 connected in parallel with L_M, having $\frac{1}{2\pi\sqrt{L_M C_3}} = f_{\rm sw}$, is proposed and the compensated circuit is named as S/SP circuit [24].

For applications requiring a load-independent output current, the value of $Z_{\rm IN}$ of the SS IPT circuit compensated using (4) is hard to determine. Here, the same circuit using the transformer M model, as shown in Fig. 5, can be readily simplified. From Fig. 5, we have

$$\dot{V}_{\rm in} = \dot{I}_p Z_P + j\omega M \dot{I}_s \tag{5}$$

$$j\omega M \dot{I}_p = -\dot{I}_s Z_S \tag{6}$$

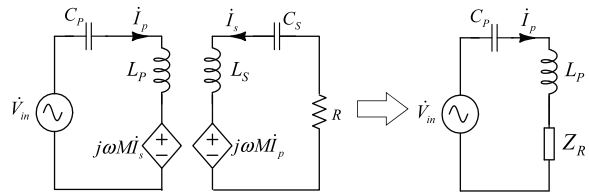

Fig. 5. SS IPT circuit in M model.

where $Z_P = j\omega L_P + \frac{1}{j\omega C_P}$ and $Z_S = j\omega L_S + \frac{1}{j\omega C_S} + R$. Then

$$Z_{\rm IN} = \frac{\dot{V}_{\rm in}}{\dot{I}_p} = Z_P + Z_R = Z_R = \frac{j\omega M \dot{I}_s}{\dot{I}_p} = \frac{\omega^2 M^2}{Z_S}. \tag{7}$$

Obviously, if C_S is designed to resonate with L_S at $f_{\rm sw}$, then Z_S and $Z_{\rm IN}$ are purely resistive, i.e.,

$$\frac{1}{2\pi\sqrt{L_S C_S}} = f_{\rm sw}. \tag{8}$$

B. SP Compensation

Similar to the analysis presented in Section II-A, the SP compensated IPT circuit shown in Fig. 6 also has two types of output characteristics. Applying compensation given by (2) and (3), the output is a load-independent current source, as shown in Fig. 6(b), with the secondary output current given by $\dot{I}_o = \frac{n\dot{V}_{\rm in}}{j\omega L_{l2}}$. Here, $Z_{\rm IN}$ can be calculated using Fig. 6(a) as follows:

$$\begin{aligned} Z_{\rm IN} &= \frac{\dot{V}_{\rm in}}{\dot{I}_{\rm in}} = j\omega L_M \| \left(\frac{j\omega L_{l2}}{n^2} + \frac{1}{j\omega n^2 C_S} \| \frac{R}{n^2} \right) \\ &= j\omega L_M \| \left(\frac{1}{n^2} \cdot \frac{1}{\omega^2 C_S^2 R - j\omega C_S} \right). \end{aligned} \tag{9}$$

Note that $Z_{\rm IN}$ in (9) is inductive, and ZPA without an additional capacitor cannot be realized.

If compensation is applied according to (4) and (8), there is no direct circuit level simplification based on the transformer T model. However, simplification can be readily obtained from the transformer M model as shown in Fig. 7. Here, the reflected impedance from secondary to primary can be calculated as

$$Z_R = \frac{j\omega M \dot{I}_s}{\dot{I}_p} = \frac{M^2 R}{L_S^2} - j\omega \frac{M^2}{L_S}. \tag{10}$$

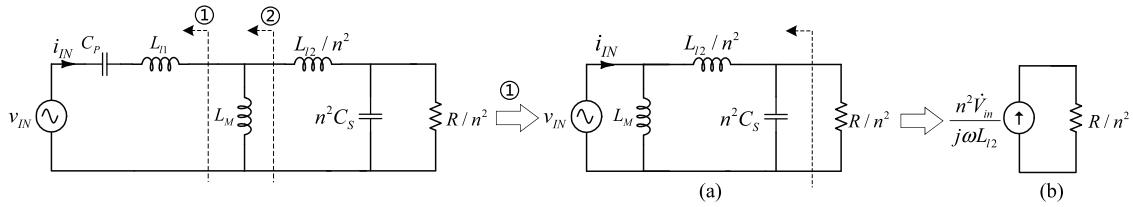

Fig. 6. IPT circuit with SP compensation and some simplified equivalent circuits (a) and (b) for current output.

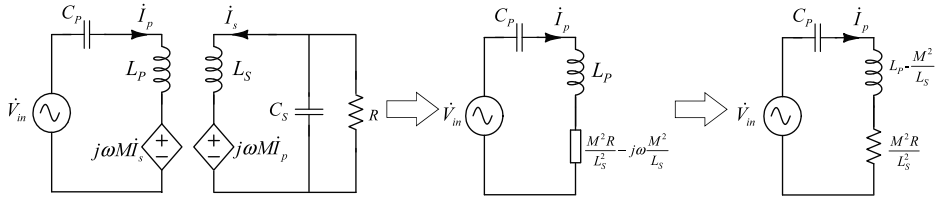

Fig. 7. SP IPT circuit using M model.

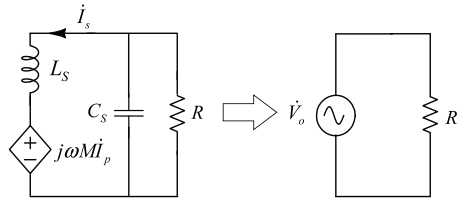

Fig. 8. Secondary equivalent circuit of SP IPT circuit using the M model.

From (10) and Fig. 7, if C_P is chosen to resonate with the inductance ($L_P - \frac{M^2}{L_S}$), then the resistive input impedance can be guaranteed, i.e.,

$$\frac{1}{2\pi\sqrt{(L_P - \frac{M^2}{L_S})C_P}} = f_{\rm sw}. \tag{11}$$

The input current i_P is thus calculated as

$$\dot{I}_p = \frac{\dot{V}_{\rm in} L_S^2}{M^2 R}. \tag{12}$$

The output voltage can be calculated using (8), (12), and Fig. 8, which is given by

$$\dot{V}_o = \frac{j\omega M \dot{I}_p}{j\omega L_S} R = \frac{L_S \dot{V}_{\rm in}}{M} \tag{13}$$

which is load independent.

C. PS and PP Compensations

PS and PP compensations have the same C_P connected in parallel with the transformer primary, which can no longer be driven by a voltage source. Thus, an additional L_X is inserted between the voltage source and the compensated primary, as shown in Fig. 9, where a PP compensated circuit has the same primary circuit shown in Fig. 10.

Figs. 9 and 10 give the equivalent circuits. Both of them are compensated by (8) and according to

$$\frac{1}{2\pi\sqrt{L_X C_P}} = f_{\rm sw}. \tag{14}$$

Then, load-independent CV and CC outputs are readily derived using circuit simplification shown in Figs. 9 and 10, i.e.,

$$\dot{V}_o = n \cdot \frac{L_M \dot{V}_{\rm in}}{L_X} = \frac{M \dot{V}_{\rm in}}{L_X}, \text{ and} \tag{15}$$

$$\dot{I}_o = \frac{1}{n} \cdot \frac{n^2 L_M \dot{V}_{\rm in}}{j\omega L_S L_X} = \frac{M \dot{V}_{\rm in}}{j\omega L_S L_X} \tag{16}$$

respectively.

To calculate the input impedances, the primary circuit in terms of the M model with a reflected impedance Z_R is used here, as shown in Fig. 11(a). The input impedance is given as

$$\begin{aligned} Z_{\rm IN} &= j\omega L_X + \tfrac{1}{j\omega C_P} \| (j\omega L_P + Z_R) \\ &= \tfrac{1}{\omega^2 C_P^2 Z_R - (1-\omega^2 L_P C_P) j\omega C_P}. \end{aligned} \tag{17}$$

Applying secondary compensation (8), the equivalent primary circuit is shown in Fig. 11(b) for PS compensation and Fig. 11(c) for PP compensation. Substituting Z_R in (17), we make $Z_{\rm IN}$ purely resistive, and we have $L_X = L_P$ for the PS compensated circuit and $L_X = L_P - \frac{M^2}{L_S}$ for the PP compensated circuit. The conditions for load-independent source and ZPA are summarized in Table I.

III. Possible Hybrid Topologies and Their Implementation as Battery Chargers

Table I summarizes the characteristics of the four compensation topologies analyzed in Section II. From this table, there is no single compensation topology that can provide ZPA for both CV and CC outputs. Therefore, appropriate switching between the two topologies is needed for CV and CC charging of the battery. For simplicity, a single transformer should be used for

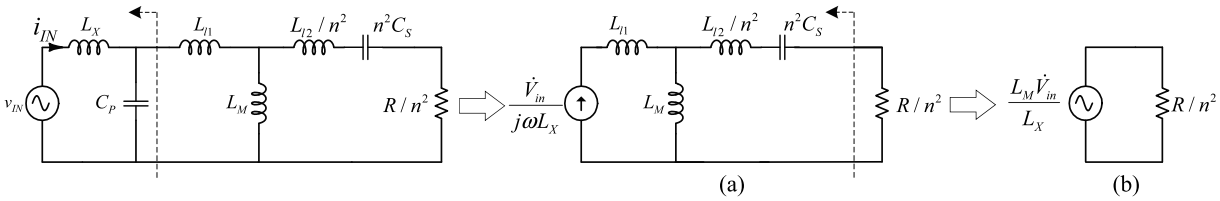

Fig. 9. IPT circuit with PS compensation and its equivalent circuits (a) and (b).

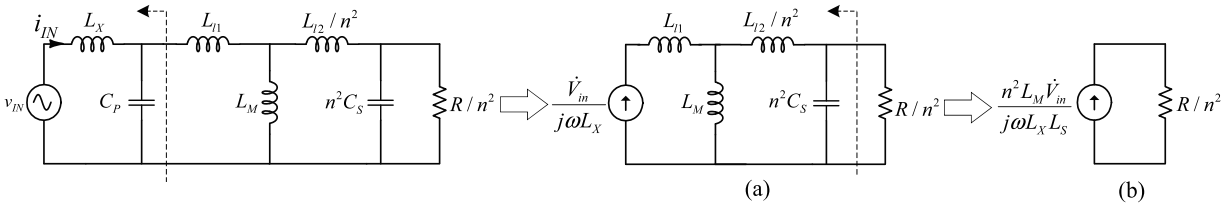

Fig. 10. IPT circuit with PP compensation and its equivalent circuits (a) and (b).

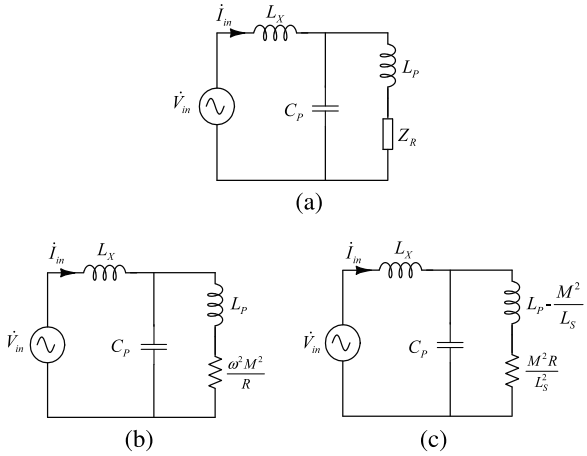

Fig. 11. (a) Equivalent primary circuits using the M model with (b) PS and (c) PP compensations.

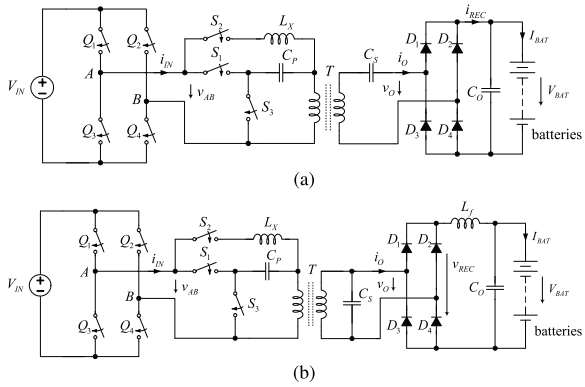

Fig. 12. Two possible hybrid IPT battery chargers: (a) Hybrid SS and PS compensated converter, and (b) hybrid SP and PP compensated converter.

the design of a hybrid CC and CV converter, with the same set of transformer parameters shown in Table I. For switching between topologies, the number of switches required for reconfiguation should be minimized. Therefore, when switching between compensation topologies, the following strategy can be adopted:

1) A single primary or secondary compensation capacitor should be used; and
2) switching of configuration should be restricted either only on the primary side or secondary side.

Hence, a hybrid SS and SP converter needs to switch between primary compensation capacitors of two different values, and also between series and parallel connection of the secondary compensation capacitor [26]. The same applies to a hybrid PS and PP converter. They will not be considered for the battery charging application in this paper.

Two possible hybrid topologies with extra three reconfiguration switches are proposed, as shown inFig. 12. Control logics for ac switches $S_{1,2,3}$ of the hybrid IPT converter operating between CC and CV modes are shown in Fig. 13. To handle bidirectional resonant currents, the ac switches should be high-frequency single-pole single-throw switches, which can be implemented with power rely, FET or BJT, such as two antiparalleled IGBTs or two antiseries MOSFETs to ensure reliable operation in each mode.

In the hybrid SS and PS compensated converter, the full-bridge switches $Q_{1,2,3,4}$ generate a square voltage v_{AB} with angle frequency $\omega = \frac{1}{\sqrt{L_P C_P}} = \frac{1}{\sqrt{L_X C_P}} = \frac{1}{\sqrt{L_S C_S}}$. When S_1 is ON, and S_2 and S_3 are OFF, it is SS compensated with $i_S = i_O = \frac{v_{\rm IN}}{\omega M}$. When S_1 is OFF, and S_2 and S_3 are ON, it is PS compensated with $v_O = \frac{M v_{\rm IN}}{L_P}$. Here, the input voltage $V_{\rm IN}$ can be modulated by $Q_{1,2,3,4}$ with D being the duty cycle of $v_{\rm AB}$. The fundamental component of $v_{\rm AB}$, denoted as $v_{\rm IN}$, is given as

$$v_{\rm IN}(t) = \frac{4V_{\rm IN}}{\pi} \sin\frac{\pi D}{2} \sin(\omega t + \theta). \tag{18}$$

Fig. 14 shows the input and output waveforms of the current and voltage of the full-bridge diode rectifier of Fig. 12 [27]. In the CC mode, the secondary current is $i_S(t) = i_O(t) = \frac{v_{\rm IN}(t)}{\omega M}$.

TABLE I
CHARACTERISTICS OF IPT CIRCUITS

Compensation circuits	Conditions	Load-independent output	ZPA
SS	$\omega = \frac{1}{\sqrt{L_P C_P}} = \frac{1}{\sqrt{L_S C_S}}$	$i_O = \frac{v_{\rm IN}}{\omega M}$	Yes
	$\omega = \frac{1}{\sqrt{L_{l1} C_P}} = \frac{1}{\sqrt{L_{l2} C_S}}$	$v_O = n v_{\rm IN}$	No
SP	$\omega = \frac{1}{\sqrt{(L_P - \frac{M^2}{L_S}) C_P}} = \frac{1}{\sqrt{L_S C_S}}$	$v_O = \frac{L_S v_{\rm IN}}{M}$	Yes
	$\omega = \frac{1}{\sqrt{L_{l1} C_P}} = \frac{1}{\sqrt{L_{l2} C_S}}$	$i_O = \frac{n v_{\rm IN}}{\omega L_{l2}}$	No
PS with L_X	$\omega = \frac{1}{\sqrt{L_P C_P}} = \frac{1}{\sqrt{L_S C_S}}$ and $L_X = L_P$	$v_O = \frac{M v_{\rm IN}}{L_P}$	Yes
PP with L_X	$\omega = \frac{1}{\sqrt{(L_P - \frac{M^2}{L_S}) C_P}} = \frac{1}{\sqrt{L_S C_S}}$ and $L_X = L_P - \frac{M^2}{L_S}$	$i_O = \frac{M v_{\rm IN}}{\omega (L_P - \frac{M^2}{L_S}) L_S}$	Yes

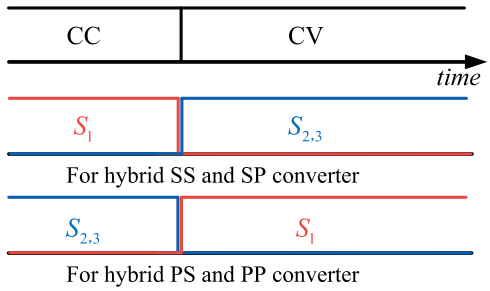

Fig. 13. Control logics for $S_{1,2,3}$ of hybrid IPT converters.

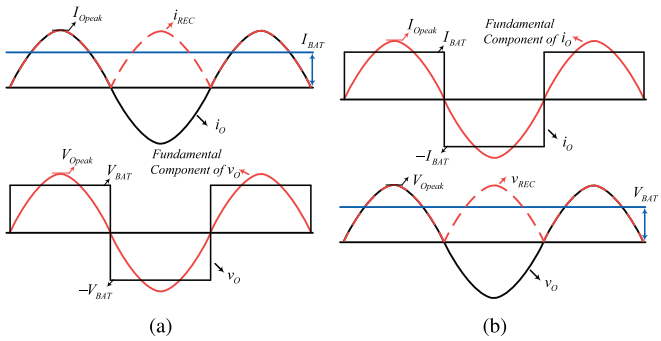

Fig. 14. Waveforms in IPT secondary rectifier for: (a) Hybrid SS and PS compensated converter, and (b) hybrid SP and PP compensated converter.

After the full-bridge rectification, the equivalent output current is given as

$$I_{\rm BAT} = \frac{2I_{O_{\rm peak}}}{\pi} = \frac{8}{\pi^2} \cdot \frac{V_{\rm IN} \sin \frac{\pi D}{2}}{\omega M}. \tag{19}$$

In CV mode, the equivalent output current with the rectification circuit is given as

$$V_{\rm BAT} = \frac{\pi V_{O_{\rm peak}}}{4} = \frac{V_{\rm IN} \sin \frac{\pi D}{2} M}{L_P}. \tag{20}$$

The hybrid SP and PP compensated converter follows a similar analysis as in Fig. 14. The output current of PP compensation is given as

$$I_{\rm BAT} = \frac{\pi I_{O_{\rm peak}}}{4} = \frac{M V_{\rm IN} \sin \frac{\pi D}{2}}{\omega (L_P - \frac{M^2}{L_S}) L_S} \tag{21}$$

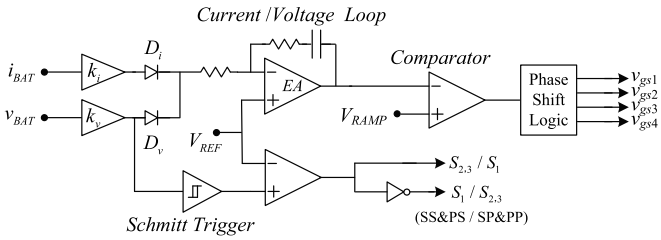

Fig. 15. Control diagram for the two hybrid IPT converters.

and the output voltage of SP compensation is given as

$$V_{\rm BAT} = \frac{2V_{O_{\rm peak}}}{\pi} = \frac{8}{\pi^2} \cdot \frac{V_{\rm IN} \sin \frac{\pi D}{2} L_S}{M}. \tag{22}$$

With specified values of $I_{\rm BAT}$ and $V_{\rm BAT}$ of a battery, the required transformer parameters M, L_P, and L_S can be calculated by (19), (20) or (21), (22) at the operating frequency. Fixed-frequency duty cycle control can readily achieve the required CC or CV output. The circuit diagram of the control is detailed in Fig. 15. Here, $k_i = \frac{V_{\rm REF}}{I_{\rm BAT}}$ and $k_v = \frac{V_{\rm REF}}{V_{\rm BAT}}$. Initially, $v_{\rm BAT} < V_{\rm BAT}$, and the IPT converter is operating in CC mode with the proper logic provided by the Schmitt trigger for the ac switches $S_{1,2,3}$. As the converter is operating in CC mode, the feedback signal $k_i i_{\rm BAT}$ can be larger than $k_v v_{\rm BAT}$, D_i is on, and D_v is reverse biased. The current loop is activated and $i_{\rm BAT}$ is regulated at the required $I_{\rm BAT}$. The voltage $v_{\rm BAT}$ is gradually increased until it reaches the required $V_{\rm BAT}$. Then, control logics of S_1 and $S_{2,3}$ are toggled and the converter is operating in CV mode. In CV mode of operation, $i_{\rm BAT}$ starts to decrease, and D_v is turned on to activate the voltage loop which ensures the output stays at the required $V_{\rm BAT}$. Some commercial ICs such as UCC3895 can implement the control logic. If the output error is small, then the variation of the duty cycle is small, which does not affect the realization of ZVS of the power switches.

IV. EXPERIMENTAL EVALUATION

To verify the above analysis, a prototype IPT battery charger with 1-A charging current and 15-V cell voltage has been built using the hybrid SS and PS compensated topology as shown in Fig. 12(a). The four switching MOSFETs are driven by a phase-shift controller UCC3895. Frequency $f_{\rm sw}$ is set at 200 kHz, and magnetics plates are Ferroxcube 3F3 ferrite core with an

TABLE II
COMPARISON OF THEORETICAL AND MEASURED TRANSFORMER PARAMETERS

Parameters	Theoretical	Experimental
L_P	24.77 μH	23.28 μH
L_S	24.77 μH	24.43 μH
M	15.48 μH	15.32 μH
L_X	24.77 μH	28.05 μH

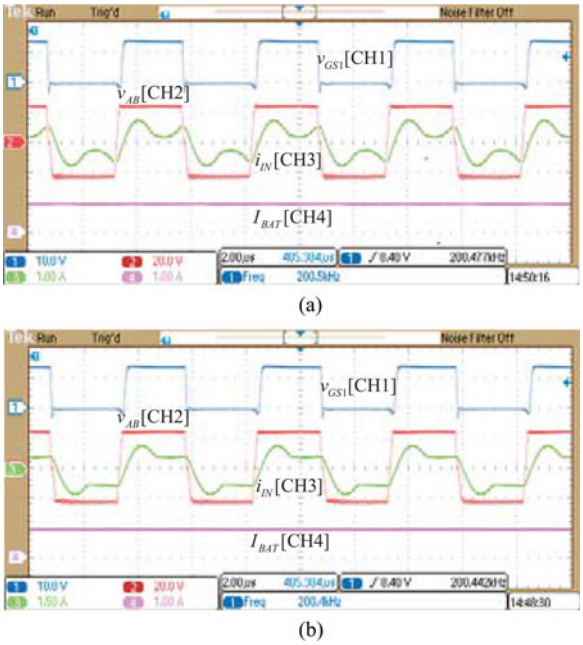

Fig. 16. Experimental waveforms of $v_{\rm GS1}$, $v_{\rm AB}$, $i_{\rm IN}$, and $I_{\rm BAT}$ in CC mode of operation with 24 V input and (a) $R_{\rm BAT} = 7\ \Omega$ or (b) $R_{\rm BAT} \approx 15\ \Omega$.

area of 60×60 mm^2 [28]. The air gap is 10 mm according to the prototype scale of the transformer. Litz wires AWG 42 with N_P : N_S of 20:20 are used. MOSFET $Q_{1,2,3,4}$ and $S_{1,2,3}$ are IRF540. The secondary rectifier diodes use MBRB3030CT. Also, C_P is 28 nF and C_S is 26.8 nF. The input voltage is 24-V dc and D is designed as 0.95. The theoretical transformer parameters are calculated using (19) and (20), which are compared with the measured transformer parameters listed in Table II. The slightly larger practical L_X permits ZVS.

Fig. 16 shows the waveforms of $v_{\rm GS1}$, the modulated voltage $v_{\rm AB}$, input current $i_{\rm IN}$ and output current $I_{\rm BAT}$ at CC mode of operation when S_1 ON and $S_{2,3}$ OFF. With $R_{\rm BAT} = \frac{v_{\rm BAT}}{i_{\rm BAT}}$ increasing from 7 Ω toward 15 Ω at $V_{\rm IN}$ =24 V, where $v_{\rm BAT}$ is increasing toward 15 V, the battery current is kept at the required 1 A independent of load variation, and $i_{\rm IN}$ is nearly in phase with v_{AB}, illustrating that reactive power has been eliminated. The small phase angle of $i_{\rm IN}$ lagging v_{AB} ensures ZVS of the full-bridge switches. When $R_{\rm BAT}$ arrives at 15 Ω, i.e., $V_{\rm BAT}$ increases to the 15-V cell voltage, the battery should be switched to CV charging by turning off S_1 and turning on $S_{2,3}$. Fig. 17 shows some key transient waveforms when the IPT converter is switching from CC to CV modes of operation. The small dead time between $v_{\rm GS\_S1}$ and $v_{\rm GS\_S3}$ allows a smooth switching

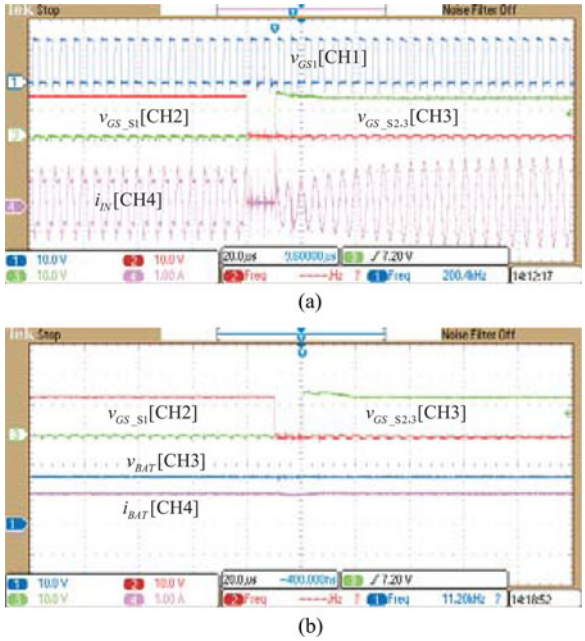

Fig. 17. Transient waveforms during CC mode to CV mode switching of $v_{\rm GS1}$, $v_{\rm GS\_S1}$, $v_{\rm GS\_S2,3}$, and the associated waveforms of (a) gate drive signal v_{GS1} and input current $i_{\rm IN}$, and (b) output $v_{\rm BAT}$ and $i_{\rm BAT}$.

between the two modes of operation. The value of $i_{\rm IN}$ increases when transiting from CC to CV modes of operation, as shown in Fig. 17(a), and the conduction loss in the primary circuit in CV mode of operation becomes larger than that in CC mode of operation. It is noted that the battery equivalent resistance $R_{\rm STR}$ varies slightly during mode switching. The output $i_{\rm BAT}$ and $v_{\rm BAT}$ change smoothly, as shown in Fig. 17(b). The steady-state waveforms of $v_{\rm GS1}$, $v_{\rm AB}$, $i_{\rm IN}$, and output voltage $V_{\rm BAT}$ in CV mode of operation are shown in Fig. 18(a) and (b) at $R_{\rm BAT}$ = 15 and 30 Ω, respectively. This also shows that CV output is achieved independent of load variation, with very little reactive power, and with ZVS for $Q_{1,2,3,4}$ in CV mode of operation.

The whole charging profile with the charging voltage and current versus time is shown in Fig. 19. The experimental data agree well with the theoretical piecewise-linear curve. The efficiency from the input to the battery in the whole charging process is measured at $V_{\rm IN} = 24$ V, as shown in Fig. 20. It can be found that the efficiency sags at the mode transition due to the increased $i_{\rm IN}$ flowing from S_1 to S_2, and the additional conduction losses in L_X and S_3.

V. CONCLUSION

IPT circuits with various kinds of compensations for load-independent battery charging are analyzed. Two hybrid topologies of SS and PS compensations, or of SP and PP compensations, using the same transformer, compensating capacitors, and operating frequency are proposed to meet the requirement of CC and CV charging without reactive power stresses on the power switches. Fixed-frequency control is readily implemented. Experimental measurements have shown good performance of the IPT charger and excellent agreement with the analysis. Although

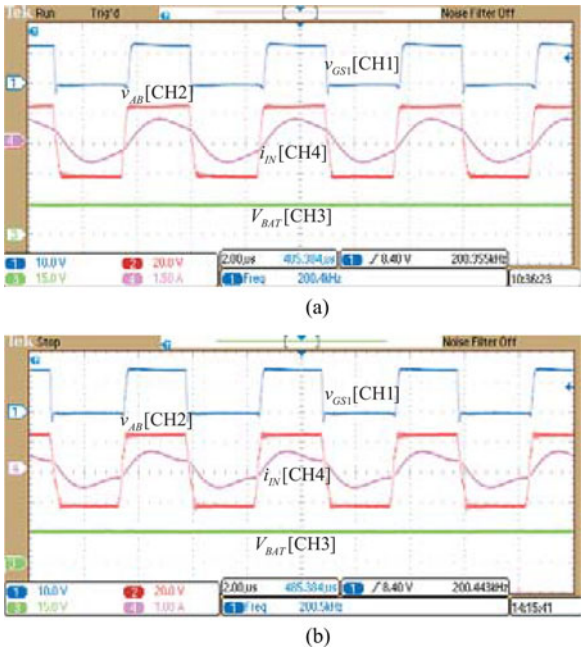

Fig. 18. Experimental waveforms of v_{GS1}, v_{AB}, i_{IN}, and V_{BAT} in CV mode of operation with 24 V input and (a) $R_{\mathrm{BAT}} = 15\ \Omega$ or (b) $R_{\mathrm{BAT}} = 30\ \Omega$.

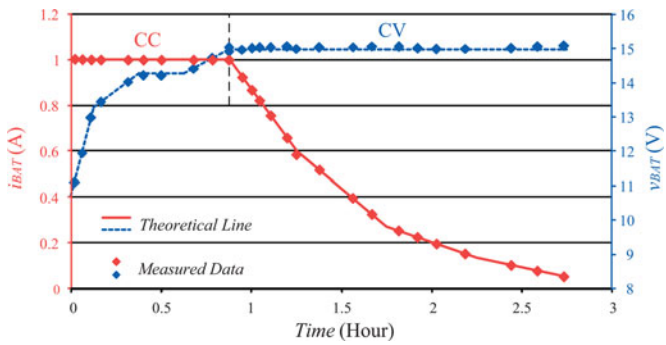

Fig. 19. Measured charing profile versus charing time.

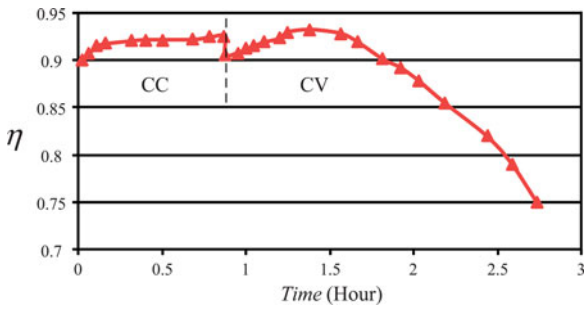

Fig. 20. Measured efficiencies of the IPT converter at CC and CV modes of charging.

these four basic compensations exhibit desirable properties for CC or CV charging, the output current or voltage gain heavily relies on transformer parameters, which are often space constrained, making the overall design hard to optimize. Higher order compensations with more freedoms on the design of current or voltage gain will be discussed in the future paper.

REFERENCES

[1] J. Sallán, J. L. Villa, and J. F. Sanz, "Optimal design of ICPT system applied to electric vehicle battery charge," *IEEE Trans. Ind. Electron.*, vol. 56, no. 6, pp. 2140–2149, Jun. 2009.

[2] W. Y. Lee, J. Huh, and S. Y. Choi, "Finite-width magnetic mirror models of mono and dual coils for wireless electric vehicles," *IEEE Trans. Power Electron.*, vol. 28, no. 13, pp. 1413–1428, Mar. 2013

[3] G. A. Covic and J. T. Boys, "Inductive power transfer," *Proc. IEEE*, vol. 101, no. 6, pp. 1276–1289, Jun. 2013.

[4] S. Lee, B. Chao, and C. T. Rim, "Dynamics characterization of the inductive power transfer system for online electric vehicles by Laplace phasor transform," *IEEE Trans. Power Electron.*, vol. 28, no. 12, pp. 5902–5909, Dec. 2013.

[5] W. Zhang, S. C. Wong, C. K. Tse, and Q. Chen, "An optimized track length in roadway inductive power transfer systems," *IEEE J. Emerging Sel. Topics Power Electron.*, vol. 2, no. 3, pp. 598–608, Sep. 2014.

[6] Y. Jang and M. M. Jovanović, "A contactless electrical energy transmission system for portable-telephone battery chargers," *IEEE Trans. Ind. Electron.*, vol. 50, no. 3, pp. 520–527, Jun. 2003.

[7] B. Choi, J. Nho, H. Cha, T. Ahn, and S. Choi, "Design and implementation of low-profile contactless battery charger using planar printed circuit board windings as energy transfer device," *IEEE Trans. Ind. Electron.*, vol. 59, no. 1, pp. 140–147, Feb. 2004.

[8] X. Liu and S. Y. Hui, "Optimal design of a hybrid winding structure for planar contactless battery charing platform," *IEEE Trans. Power Electron.*, vol. 23, no. 1, pp. 455–463, Jan. 2008.

[9] S. Y. Hui, "Planar wireless charging technology for portable electronic products and Qi," *Proc. IEEE*, vol. 101, no. 6, pp. 1290–1301, Jun. 2013.

[10] H. H. Wu, J. Boys, G. Covic, and D. Robertson, "A practical 1.2 kW inductive power transfer lighting system using AC processing controllers," in *Proc. IEEE Conf. Ind. Electron. Appl.*, 2011, pp. 345–350.

[11] J. E. James, A. Chu, A. Sabitov, D. Robertson, and G. Covic, "A series tuned light power IPT stage lighting controller," in *Proc. IEEE Energy Convers. Congr. Expo.*, 2011 pp. 2843–2849.

[12] 3I Innovation Inc. (2015). Inductively powered LED lighting solutions. [Online]. Available: http://www.3iinnovation.com/

[13] G. A. Covic and J. T. Boys, "Modern trends in inductive power transfer for transportation applications," *IEEE J. Emerging Sel. Topics Power Electron.*, vol. 1, no. 1, pp. 28–41, Mar. 2013.

[14] C. Chen, S. C. Wong, C. K. Tse, and X. Ruan, "Analysis, design, and control of a transcutaneous power regulator for artificial hearts," *IEEE Trans. Biomed. Circuits Syst.*, vol. 3, no. 1, pp. 23–31, Feb. 2009.

[15] C. S. Wang, O. H. Stielau, and G. A. Covic, "Design considerations for a contactless electric vehicle battery charger," *IEEE Trans. Ind. Electron.*, vol. 52, no. 5, pp. 1308–1314, Oct. 2005.

[16] M. Budhia, G. A. Covic, and J. T. Boys, "Design and optimization of circular magnetic structures for lumped inductive power transfer systems," *IEEE Trans. Power Electron.*, vol. 26, no. 11, pp. 3096–3108, Nov. 2014.

[17] C. S. Wang, G. A. Covic, and O. H. Stielau, "Power transfer capability and bifurcation phenomena of loosely coupled inductive power transfer systems," *IEEE Trans. Ind. Electron.*, vol. 51, no. 1, pp. 148–157, Feb. 2004.

[18] Z. Pantic, S. Bai, and S. M. Lukic, "ZCS LCC-compensated resonant inverter for inductive-power-transfer application," *IEEE Trans. Ind. Electron.*, vol. 58, no. 8, pp. 3500–3510, Aug. 2011.

[19] W. Zhang, S. C. Wong, and C. K. Tse, "Analysis and comparison of secondary series- and parallel-compensated inductive power transfer systems operating for optimal efficiency and load-independent voltage-transfer ratio," *IEEE Trans. Power Electron.*, vol. 29, no. 6, pp. 2979–2990, Jun. 2014.

[20] W. Zhang, S. C. Wong, and C. K. Tse, "Design for efficiency optimization and voltage controllability of series-series compensated inductive power transfer systems," *IEEE Trans. Power Electron.*, vol. 29, no. 1, pp. 191–200, Jan. 2014.

[21] W. Zhang, S. C. Wong, C. K. Tse, and Q. Chen, "Load-independent current output of inductive power transfer converters with optimized efficiency," in *Proc. Int. Power Electron. Conf.*, 2014, pp. 1425–1429.

[22] X. Qu, S. C. Wong, C. K. Tse, and G. Zhang, "Design Consideration of a current-source-output inductive power transfer LED lighting system," in *Proc. IEEE Energy Convers. Congr. Expo.*, 2014, pp. 3607–3611.

[23] M. L. G. Kissin, J. T. Boys, and G. A. Covic, "Interphase mutual inductance in polyphase inductive power transfer systems," *IEEE Trans. Ind. Electron.*, vol. 56, no. 7, pp. 2393–2400, Jul. 2009.

[24] J. Hou, C. Chen, K. Yan, X. Ren, S. C. Wong, and C. K. Tse, "Analysis and control of S/SP compensation contactless resonant converter with constant voltage gain," in *Proc. IEEE Energy Convers. Congr. Expo.*, 2013 pp. 2552–2558.
[25] Z. Huang, S. C. Wong, and C. K. Tse, "Design methodology of a series-series inductive power transfer system for electric vehicle battery charger application," in *Proc. IEEE Energy Convers. Congr. Expo.*, 2014 pp. 1778–1782.
[26] C. Auvigne, P. Germano, D. Ladas, and Y. Perriard, "A dual-topology ICPT applied to an electric vehicle battery charger," in *Proc. Int. Conf. Electr. Mach.*, 2012 pp. 2287–2292.
[27] R. W. Erickson and D. Maksimović, *Fundamentals of Power Electronics*. Norwell, MA, USA: Kluwer, 2001.
[28] Ferroxcube Inc. (2008). 3F3 material specification. [Online]. Available: http://www.ferroxcube.com/FerroxcubeCorporateReception/datasheet/3f3.pdf

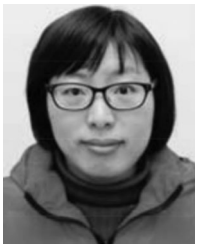

Xiaohui Qu (S'08–M'10) received the B.Sc. and M.Sc. degrees in electrical engineering from the Nanjing University of Aeronautics and Astronautics, Nanjing, China, in 2003 and 2006, respectively, and the Ph.D. degree in power electronics from the Hong Kong Polytechnic University, Hung Hom, Hong Kong, in 2010.

From February to May 2009, she was a Visiting Scholar with the Center for Power Electronics Systems, Virginia Tech, Blacksburg, VA, USA. Since April 2010, she has been a Lecturer with the School of Electrical Engineering, Southeast University, Nanjing. Her current research interests include LED lighting systems, wireless power transfer, power factor correction preregulators, and resonant converters.

Hongdou Han received the B.Sc. degree in electrical engineering from the Nanjing University of Technology, Nanjing, China, in 2013. He is currently working toward the M.Sc. degree in electrical engineering at Southeast University, Nanjing.

His current research interest includes wireless power transfer in EV charing and LED lighting systems.

Siu-Chung Wong (M'01–SM'09) received the B.Sc. degree in physics from the University of Hong Kong, Pok Fu Lam, Hong Kong, in 1986, the M.Phil. degree in electronics from the Chinese University of Hong Kong, in 1989, and the Ph.D. degree from the University of Southampton, Southampton, U.K., in 1997.

In 2012, he was appointed as a Chutian Scholar Chair Professor at the Hubei Provincial Department of Education, China, and the appointment was hosted by the Wuhan University of Science and Technology, Wuhan, China. In 2013, he was appointed as a Guest Professor by the School of Electrical Engineering, Southeast University, Nanjing, China. He was a Visiting Scholar at the Center for Power Electronics Systems, Virginia Tech, Blacksburg, VA, USA, on November 2008; Aero-Power Sci-Tech Center, Nanjing University of Aeronautics and Astronautics, Nanjing, on January 2009, and; the School of Electrical Engineering, Southeast University, Nanjing, on March 2012. In 1988, he joined the Hong Kong Polytechnic University, Hung Hom, Hong Kong, as an Assistant Lecturer, where he is currently an Associate Professor at the Department of Electronic and Information Engineering, where he conducts research in power electronics.

Dr. Wong is a Member of the Electrical College, The Institution of Engineers, Australia. He is an Editor of the *Energy and Power Engineering Journal* and a Member of the Editorial Board of the *Journal of Electrical and Control Engineering*.

Chi K. Tse (M'90–SM'97–F'06) received the B.Eng.(with first class Hons.) degree in electrical engineering and the Ph.D. degree from the University of Melbourne, Parkville, Vic., Australia, in 1987 and 1991, respectively.

From 2005 to 2012, he was the Head of Department of Electronic and Information Engineering with the Hong Kong Polytechnic University, Hung Hom, Hong Kong, where he is currently a Chair Professor of electronic engineering. His research interests include complex network applications, power electronics, and nonlinear systems.

Dr. Tse serves as an Editor-in-Chief of the IEEE CIRCUITS AND SYSTEMS MAGAZINE and an Editor-in-Chief of the IEEE CIRCUITS AND SYSTEMS SOCIETY NEWSLETTER. He was/is an Associate Editor for the IEEE TRANSACTIONS ON CIRCUITS AND SYSTEMS PART I—FUNDAMENTAL THEORY AND APPLICATIONS from 1999 to 2001, and again from 2007 to 2009. He has also been an Associate Editor for the IEEE TRANSACTIONS ON POWER ELECTRONICS since 1999. He is an Editor of *International Journal of Circuit Theory and Applications* and on the Editorial Boards of a few other journals. He received the Best Paper Award from the IEEE TRANSACTIONS ON POWER ELECTRONICS in 2001 and the Best Paper Award from the *International Journal of Circuit Theory and Applications* in 2003. In 2005 and 2011, he was selected and appointed as the IEEE Distinguished Lecturer. In 2007, he received the Distinguished International Research Fellowship by the University of Calgary, Canada. In 2009 and 2013, he and his coinventors won the Gold Medal at the International Exhibition of Inventions of Geneva, Switzerland, on LED lighting technologies. In 2011, he was appointed as the Honorary Professor by the RMIT University, Melbourne, Australia. In 2013 and 2015, he received the Gledden Fellowship and the Distinguished International Fellowship by the University of Western Australia, Perth, Australia.

Wu Chen (S'05–M'12) received the B.Sc., M.Sc., and Ph.D. degrees in electrical engineering from the Nanjing University of Aeronautics and Astronautics, Nanjing, China, in 2003, 2006, and 2009, respectively.

From 2009 to 2010, he was a Senior Research Assistant with the Department of Electronic Engineering, City University of Hong Kong, Kowloon, Hong Kong. From 2010 to 2011, he was a Postdoctoral Researcher with the Future Electric Energy Delivery and Management Systems Center, North Carolina State University, Raleigh. Since September 2011, he has been an Associate Research Professor with the School of Electrical Engineering, Southeast University, Nanjing. His main research interests include soft-switching converters, microgrid, and power electronic application.